

Contents lists available at ScienceDirect

BBA - Biomembranes

journal homepage: www.elsevier.com/locate/bbamem





The stressed life of a lipid in the Zika virus membrane

Martín Soñora a, Exequiel E. Barrera a,b, Sergio Pantano a,*

- ^a Biomolecular Simulations Group, Institut Pasteur de Montevideo, Mataojo 2020, CP 11400 Montevideo, Uruguay
- b Instituto de Histología y Embriología (IHEM) Consejo Nacional de Investigaciones Científicas y Técnicas (CONICET), CC56, Universidad Nacional de Cuyo (UNCuyo), Mendoza, Argentina

ARTICLE INFO

Keywords: Zika virus Flavivirus SIRAH VLP Coarse-grain Molecular dynamics Simulation

ABSTRACT

Protein-lipid interactions modulate a plethora of physiopathologic processes and have been the subject of countless studies. However, these kinds of interactions in the context of viral envelopes have remained relatively unexplored, partially because the intrinsically small dimensions of the molecular systems escape to the current resolution of experimental techniques. However, coarse-grained and multiscale simulations may fill that niche, providing nearly atomistic resolution at an affordable computational price.

Here we use multiscale simulations to characterize the lipid-protein interactions in the envelope of the Zika Virus, a prominent member of the *Flavivirus* genus. Comparisons between the viral envelope and simpler molecular systems indicate that the viral membrane is under extreme pressures and asymmetric forces. Furthermore, the dense net of protein-protein contacts established by the envelope proteins creates poorly solvated regions that destabilize the external leaflet leading to a decoupled dynamics between both membrane layers. These findings lead to the idea that the Flaviviral membrane may store a significant amount of elastic energy, playing an active role in the membrane fusion process.

1. Introduction

Since the postulation of phospholipids as the basis of biological membranes in 1935 by Danielli and Davson [1], and the proposal of the fluid mosaic model in 1972 by Singer and Nicolson [2], great advances have contributed to deepening our knowledge of the structure and dynamics of membrane-protein interactions [3–5]. For example, today is clear that membrane-associated cytoskeletal networks and extracellular matrix structures limit lateral diffusion of lipids to nanometer-sized compartments [5,6]. Moreover, the rich and dynamic heterogeneity of components that make up biological membranes and their interactions, makes this field fascinating [7–11]. A nice summary about the main features of the Fluid membrane model and how it evolved to our current understanding of bio-organic membranes was recently provided by Felix Goñi [12].

Historically, technological developments have led major break-throughs. For instance, super-resolution imaging granted unprecedented details on membrane heterogeneity and dynamics [13–15], and single-molecule imaging was crucial to characterize the kinetics for transient lipid-protein interactions [16]. Similarly, NMR spectroscopy provided great insights on membrane proteins and details on lipid-protein

interfaces [17,18].

More recently, the astonishing developments of cryoelectron microscopy (CryoEM) and tomography have revolutionized structural biology by offering 3D protein information and large macromolecular assemblies at resolutions comparable to those of X-ray crystallography but outside the crystalline environment [19,20].

Worth mentioning, molecular dynamics (MD) simulations have become an outstanding tool for exploring the processes of biological systems and for understanding the underlying mechanisms. MD simulations have contributed a complementary view on the structure and dynamics of membrane systems connecting the nano with the *meso* scales and achieving an impressive level of complexity [21–26].

Nevertheless, our understanding of the lipid-protein interplay in viral systems is considerably more limited. Although it is well established that viruses interact with specific lipids to mediate fusion, entry, and also reprogram the host-cell metabolism [20], their small size continues to hamper a highly detailed knowledge of their membrane dynamics and lipid-protein interactions in intact virions. This is particularly the case for small-enveloped viruses such as Zika Virus and other *Flaviviruses*, which are close to or below the lower resolution limits of many experimental techniques. Also, MD techniques may encounter

E-mail address: spantano@pasteur.edu.uy (S. Pantano).

^{*} Corresponding author.

serious difficulties in studying entire viral particles because of the high computational cost associated with the simulations. Indeed, despite the ever-increasing computational power and cutting-edge simulation algorithms, only a few dozens of simulations of whole virions or Virus-like particles (VLP) have been reported in the literature [27]. In this context, coarse-grained (CG) and multiscale methods applied to the simulation of virions have become a powerful alternative to fully atomistic simulations [28–32].

In this contribution, we aim at providing fresh insights into the lipidprotein interactions within the Zika Virus (ZIKV) envelope by performing a comparative analysis of CG simulations on different membrane environments.

ZIKV belongs to the family Flaviviridae, genus Flavivirus. They are enveloped viruses with a single-stranded RNA genome of positive polarity transmitted to humans by arthropods. Other prominent members of the genus include Dengue Virus (DENV), Yellow Fever Virus (YFV), West Nile Virus (WNV), and Japanese Encephalitis Virus (JEV), which share similarities in virion morphology, genome organization, and replication strategies [33]. The mature form of the virion includes a single copy of the genetic material and three structural proteins, namely, the Nucleocapsid, Membrane (M), and Envelope (E) proteins. While the number of Nucleocapsids has not been determined, mature virions contain 180 copies of membrane-anchored heterodimers of E and M. E-M complexes associate into dimers of heterodimers that feature four double-pass transmembrane (TM) segments and six amphipathic, or stem helices that connect to the E's ectodomains (Fig. 1A). These protein complexes introduce variations in the thickness and a curvature of the membrane that ultimately results in a closed envelope with the ectodomains covering the viral membrane to produce an icosahedrally symmetric virion [34]. CryoEM structures of ZIKV (Fig. 1B) and other Flaviviruses showed that each of the faces of the icosahedron is composed of three dimers of heterodimers [19,35], which are called "rafts" (not to be confused with cholesterol-rich lipid rafts).

We aim at characterizing the ZIKV's VLP lipid-protein interactions in comparison with simpler membrane systems (Fig. 2). To this goal, we compare lipid-lipid and lipid-protein interactions in CG simulations of a planar lipid bilayer (hereafter named patch), a protein-free vesicle, and a planar bilayer containing an ER protein pentamer. To the ends of the comparison, we selected the pentamer of the protein Phospholamban (PLB). Besides inhibiting the SarcoEndoplasmic Reticulum Calcium (SERCA) pump [36], this protein forms stable pentamers in the ER membrane [37]. PLB feature a highly mobile cytoplasmic helix and a TM motif that mediate their association (Fig. 2C), leaving only their C-termini exposed to the ER lumen. This ER protein was arbitrarily selected because of our previous experiences with this system [36,38]. Finally, a vesicle containing six PLB pentamers was also simulated to complete the different scenarios considered.

The information about the detailed composition of the Zika Virus envelope is scarce. Moreover, matching the large lipid diversity is highly challenging for MD simulations. Therefore, we adopted a minimalist composition of only three different lipids already presented in the literature [39,40]. As detailed in the Methods section, our simplistic version of the ZIKV envelope contains only 1-Palmitoyl-2-Oleoyl-sn-Glycero-3-Phosphocholine (POPC), 1-Palmitoyl-2-Oleoyl-sn-Glycero-3-Phosphoethanolamine (POPE), and 1-Palmitoyl-2-Oleoyl-sn-Glycero-3-Phospho-1-Serine (POPS). These three lipids are meant to represent phospholipids with different physicochemical characteristics. Namely, they are used to represent big and small polar heads and anionic lipids, respectively, rather than a specific molecule. This shortcoming clearly constitutes a limitation in our study that is important to keep in mind.

A comparison of structural and dynamic descriptors in these systems indicates that the quaternary structure of the VLP, as a whole, imposes severe stress conditions on the lipids in the viral envelope. In addition to the thickness heterogeneity evidenced from several CryoEM structures, our simulations suggest that lipids in the viral envelope move under extreme compressions that induce different dynamical states in the inner

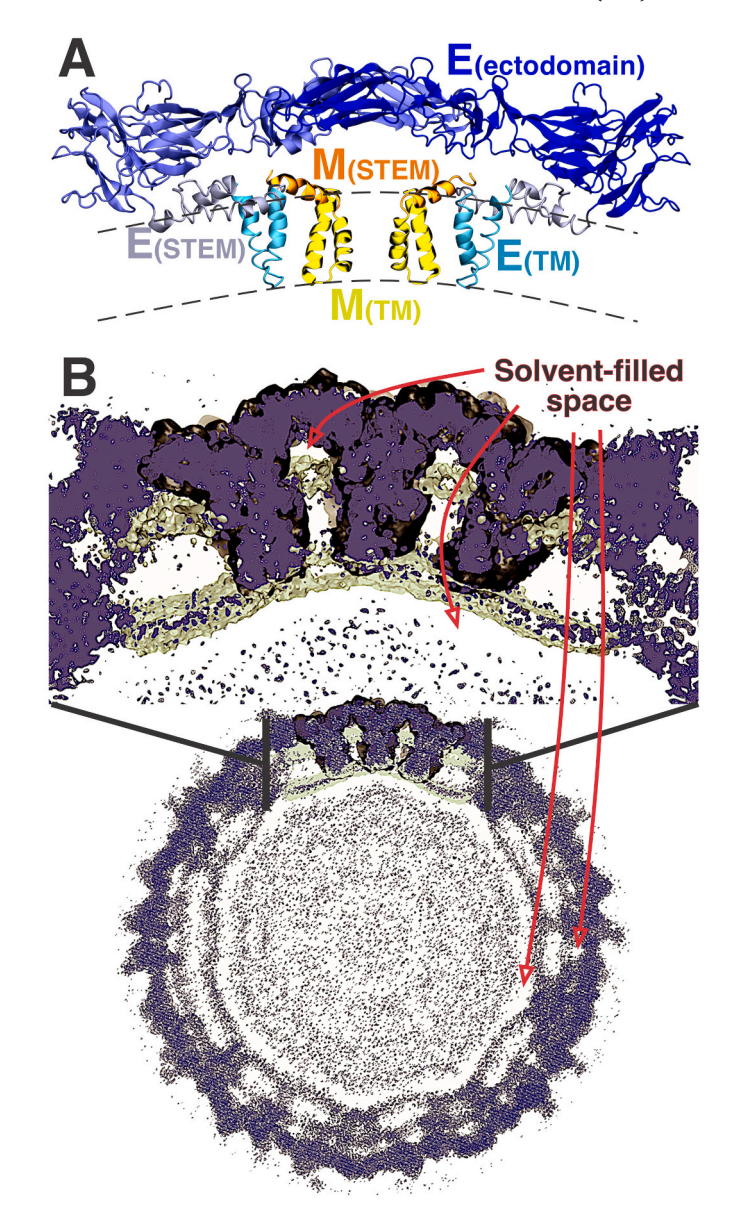


Fig. 1. Structure of the Zika Virus. A) Dimer of E-M heterodimers. The protein regions relevant to this work are indicated in different colors. Dashed lines indicate the approximate position of the membrane. Three dimers associate to form a "protein raft". B) Electron density map of the Zika Virus obtained by CryoEM [19]. The inset shows the superposition between the experimental and simulated densities in a protein raft [31]. Black and lime colors highlight the regions corresponding to the protein and membrane, respectively.

and outer leaflets.

2. Methods

All simulations analyzed in this study were carried out using the SIRAH force field for CG and multiscale simulations, which grants over two orders of magnitude in speed up compared to fully detailed simulations keeping nearly atomistic resolution [41] and providing an accurate representation of the mechanical properties of lipid systems [42]. Some of the CG simulations analyzed here have been previously published. We refer the interested readers to those publications for full simulation details.

Our study is based on the molecular systems described below.

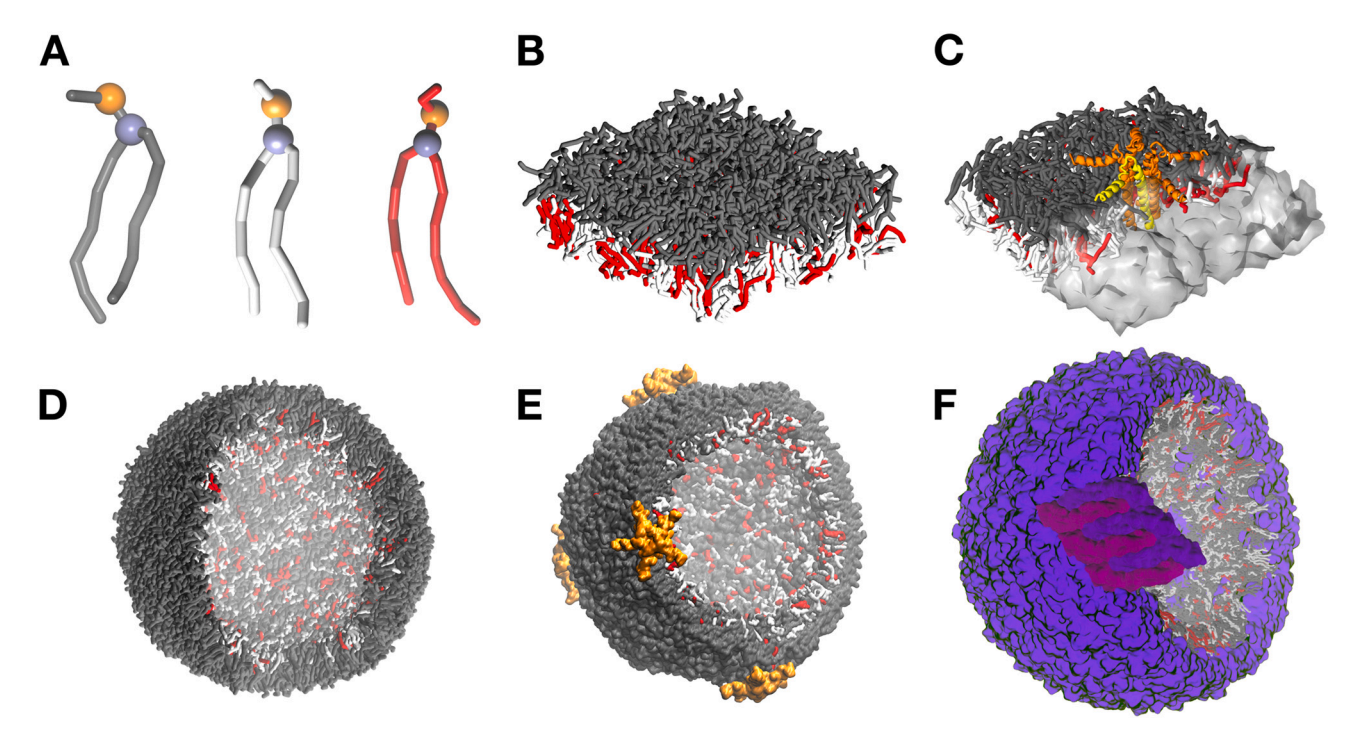


Fig. 2. Different systems studied in this work. A) CG phospholipids composing the membranes (POPC: dark gray, POPE: light gray, POPS: red). Orange and blue beads indicate the position of the phosphate and glycerol moieties used to measure different properties, such as mobility and contacts. B) Flat membrane patch. C) Flat membrane patch with a pentamer of PLB inserted. One protein chain is shown in yellow, and half of the membrane patch is shown as semitransparent to facilitate the visualization. D) Lipid vesicle. E) Lipid Vesicle with six pentamers of PLB. F) Representation of the ZIKV with the proteinaceous envelope covering the membrane (indigo). One protein raft, composed of three dimers of E-M heterodimers, is evidenced on the surface in purple tones. (For interpretation of the references to color in this figure legend, the reader is referred to the web version of this article.)

2.1. Simple bilayers

The flat membrane patch and the PLB systems were published in [38]. Briefly, they are constituted by flat membranes of 14 nm by 14 nm containing POPC in one side of the membrane and a mix of POPE:POPS in a 65% and 35% ratio in the other (Fig. 2A, B). The PLB pentamer, corresponding to the PDB structure 2KYV, was inserted in the membrane, and overlapping lipids were removed (Fig. 2C). The atomistic structure was mapped to CG resolution by using SIRAH Tools [43]. Both systems underwent 5000 iterations of energy minimization using the steepest descent algorithm and equilibrated to 310 K and 1 atm with semi-isotropic pressure coupling using Berendsens' thermostat and barostat during 15 ns with a timestep of 20 fs. During the first step, we applied positional restraints in z coordinate over the phosphate beads of 100 kJ/mol·nm² and protein's beads restraints of 1000 kJ/mol·nm². In the second equilibrating round, we used restraints over phosphate beads of 100 kJ/mol·nm² in x, y, and z and protein backbone restraints of 100 kJ/mol·nm².

To determine the lateral pressure of rupture of flat membrane bilayers, we constructed and simulated three types of membranes composed of POPC, POPE, and a mixture of POPC:POPE:POPS in a 6:3:1 proportion, following the same procedure described above. After the first microsecond of simulation, we coupled the membrane patches to increasing lateral pressures using a semi-isotropic coupling scheme. Simulations were performed keeping the perpendicular pressure to 1 bar and increasing the lateral coupling by 5 bars in intervals of 0.5 μs until we observed the rupture of the bilayer.

For the PLB system, additional equilibration steps with positional constraints on the protein beads were implemented. The production phase was performed for 2 μ s at 310 K, saving frames every 5000 steps, using a V-rescale thermostat [44] and 1 bar under semi-isotropic couplings using Parrinello-Rahman barostat [45].

This procedure leads to a smooth stabilization of the VLP with

maximum errors from the experimental radius of gyration below 2%. It also allows for a sensible improvement in the correlation between measured and simulated density maps already in the stabilization phase (Supplementary Fig. S1).

2.2. Vesicle system

Because of computational efficiency, the lipid vesicle was built up using the multiscale solvation scheme previously reported by us [31,32]. This method uses two water models with different granularities. CG water molecules (representing nearly 11 atomistic water molecules) were used to generate a solvation shell near the vesicle; while a supra-CG model (representing 55 atomistic water molecules) was used to account for the large amount of bulk solvent present in the inner core of the vesicles and the outmost regions of simulation boxes. These models have been exhaustively tested and provide the best compromise between computational cost and structural accuracy for highly solvated systems [32].

To preserve the spherical shape of the vesicle, only POPC molecules, which favor convex geometries, were placed in the outer leaflet, while the POPC, POPE, and POPS were placed in the inner leaflet in a 6:3:1 proportion to mimic that used for ZIKV (see below). The setup protocol for assembling the vesicle was identical to that introduced by us for VLPs [31] and included the following steps:

i) Lipids were initially ordered in spherical geometry with a diameter of 30 nm using Packmol [46] and placed in a truncated octahedron computational box extending up to 7.5 nm apart from the lipids in all directions. ii) A 2.5 nm shell of CG water close to the inner leaflet was added, and sodium ions were used to neutralize the negative charges of the POPS molecules. iii) A 2.5 nm shell of CG water apposed to the outer leaflet was added. iv) The inner core and outmost regions of the computational box were filled with supra-CG water.

To achieve a gradual relaxation, we followed a multi-step strategy of

minimization and equilibration steps. We first performed 5000 iterations of the steepest descent algorithm to minimize the global energy of the system. Then, an NPT equilibration step using: simulation time = 100 ps, time step = 2 fs. After the first equilibration, re-solvation with CG water was necessary to fill void spaces formed due to small unbalances in the initial densities. The energy was minimized again, and a second equilibration dynamics with simulation time = 2 ns, time step = 10 fs, positional restraints = 1000 kJ/mol.nm^2 applied on phosphate beads. Subsequently, a third equilibration using simulation time = 5 ns, time step = 20 fs. The temperature was kept at 310 K in all steps using the V-rescale Thermostat [44], and a pressure of 1 bar was controlled isotropically using the Berendsen's barostat [47]. The Vesicle system was simulated to achieve 2 μ s production under isotropic Parrinello-Rahman coupling conditions, saving frames every 5000 steps, using the Molecular Dynamics software GROMACS 2018 [48,49].

2.3. Vesicle-PLB system

We used the final snapshot of the 2 µs vesicle trajectory to insert equidistantly on the bilayer six copies of the PLB pentamer (PDB ID: 2KYV). Overlapping lipids were removed. Energy was minimized performing 5000 steps of the steepest descent algorithm. Four NPT equilibration steps were performed as follows: Step 1) simulated time = 100 ps; time steps = 2 fs; positional restraints = $1000 \text{ kJ/mol} \cdot \text{nm}^2$ on the inner leaflet phosphate beads and protein's backbone. Step 2) simulated time = 1 ns; time steps = 20 fs; positional restraints = $100 \text{ kJ/mol} \cdot \text{nm}^2$ on all the phosphate beads and 1000 kJ/mol·nm² on the protein's backbone. Step 3) simulated time = 1 ns; time steps = 20 fs; positional restraints = $1000 \text{ kJ/mol} \cdot \text{nm}^2$ on the protein's backbone. Step 4) simulated time = 10 ns; time steps = 20 fs; positional restraints = 100kJ/mol·nm² on the protein's backbone. In all four steps, temperature was kept at 310 K and pressure at 1 atm using the V-rescale thermostat [44] and Berendsen barostat [47], respectively. The vesicle-PLB system was simulated for 1 µs under isotropic Parrinello-Rahman coupling conditions.

2.4. ZIKV System

The simulation of the Zika Virus' VLP is based on the high-resolution structure of the mature virion (PDB: 6CO8 [19]). Because of the size and intrinsic complexities of this large molecular assembly, the building up and stabilization of this system is intricate and involves several steps of solvation, stabilization, and resolvation. The entire protocol has been very recently reported by us [31]. The number of lipids was set according to experimental estimation for the closely related West Nile Virus [34]. We used a 6:3:1 proportion of POPC, POPE, and POPS, respectively, in rough correspondence with the lipid content of the ER [50] and previous simulation studies [39].

The production simulations were performed under similar conditions to the previous systems with two differences: First, the target temperature of the ZIKV system was set to 300 K, i.e., the temperature of the *Aedes aegypti* mosquito that transmits the virus, while the temperature in all other systems was set to 310 K, to match that of humans. Second, in the membrane patches and vesicle system, the lipidic composition is asymmetric in both leaflets. In contrast, the phospholipids in the VLP are symmetrically distributed in the inner and outer leaflets. The rationale for this choice is that, in living cells, there are active systems that ensure the lipidic partition [51]. Since such systems are absent in the viral envelope, we assumed an even distribution at both sides of the bilayer.

2.5. Analyzed properties

Areas per lipid (APL) were calculated with FATSLiM [52]. Diffusion coefficients in the PLB and ZIKV systems were calculated with the Einstein relation from the mean square displacement of phosphate beads using the Gromacs' utility gmx msd [49]. In the case of ZIKV, the

diffusion was calculated on the lipids beneath a protein raft. For that, the coordinates of lipids within 4 nm of any protein bead were selected from snapshots recorded every nanosecond of simulation, and a new trajectory was created using Gromacs' utilities. Lipid-Lipid and Lipid-Protein contacts were computed using Gromacs engine, gmx mindist software [49], using a cut-off distance of 1.1 nm between glycerol beads or glycerol-C α carbon beads. Phosphate and glycerol beads used to measure different quantities are indicated by spheres in Fig. 2A.

Vibrational normal modes by principal component analysis of POPS were calculated with PCALipids [53] over 100 ns of equilibrated trajectories for the PLB and ZIKV systems. The study included the generation of atomic displacement covariance matrices, their eigenvectors, and eigenvalues. Eigenvectors of different systems were compared, calculating their dot product matrix. Distributions of projections on principal components and all molecular representations were visualized with VMD [54].

Instantaneous displacement measurement was conducted by Flows [55] at different simulation points (at 0.5, 1.0, 1.5, and 2.0 μ s) of the ZIKV system. Lipids were selected using the same strategy adopted to calculate the diffusion coefficients (see above).

3. Results

The mature forms of ZIKV and other *Flaviviruses* have been solved by CryoEM. However, atomic resolution was only achieved for the proteinaceous envelope, constituted by 180 copies of *E*-M heterodimers. The electron density of the whole virion is accurate enough to evidence regions depleted from electron density below the membrane and in specific places between the membrane and the ectodomain of protein E (Fig. 1B).

An accurate description of the building up of the VLP containing lipids and solvent and the corresponding CG simulation was recently reported by us [31].

Aimed to establish comparative references between the structural characteristics of ZIKV's lipid envelope, we analyzed the physicochemical properties of membranes mimicking different biophysical environments depicted in Fig. 2. Notice that not all the comparisons are possible because the lipid distribution is not even in the various systems.

APLs are salient structural properties of lipid bilayers that can describe the state of stress of membrane surfaces. As the environment's physicochemical characteristics may modify APLs, we sought to perform a comparative study in the environments depicted in Fig. 2.

A comparative view of the APLs for the different lipids and systems is presented in Fig. 3. Because of the heterogeneity in lipid contents in both leaflets, the comparison is shown only whenever possible for all three phospholipids.

It is immediate to notice that the restrictions imposed by the virus' quaternary structure induce a considerable lateral shrinkage in all phospholipid species and regardless of their location in the outer or inner leaflets (Fig. 3A). In the case of POPC (Fig. 3A, top panel), the comparison between the flat membrane patches in the absence and presence of PLB proteins indicates that the protein's presence induced a shift to lower values while grossly preserving the shape of the distribution. This effect is emphasized in the ZIKV's VLP, where POPC suffers a further APL reduction. In contrast, the convexity of the vesicle's outer surface and the absence of proteins cooperate to confer to POPC the highest APL with the narrowest dispersion. The presence of six copies of PLB pentamer on the vesicle partially compensated for this effect (Fig. 3A), inducing a slight but clear shrinkage of APLs of POPC present in the outer leaflet.

In the inner leaflet, POPE and POPS experience a progressive shrinkage in passing from the flat patch to PLB, the vesicle, and the VLP (Fig. 3A, middle and lower panels). Therefore, the concavity/convexity of the surface acts in opposite ways, shrinking or stretching the areas per lipid. At the same time, the presence of the PLB pentamer and the viral envelope contribute to increasing the membrane's compaction.

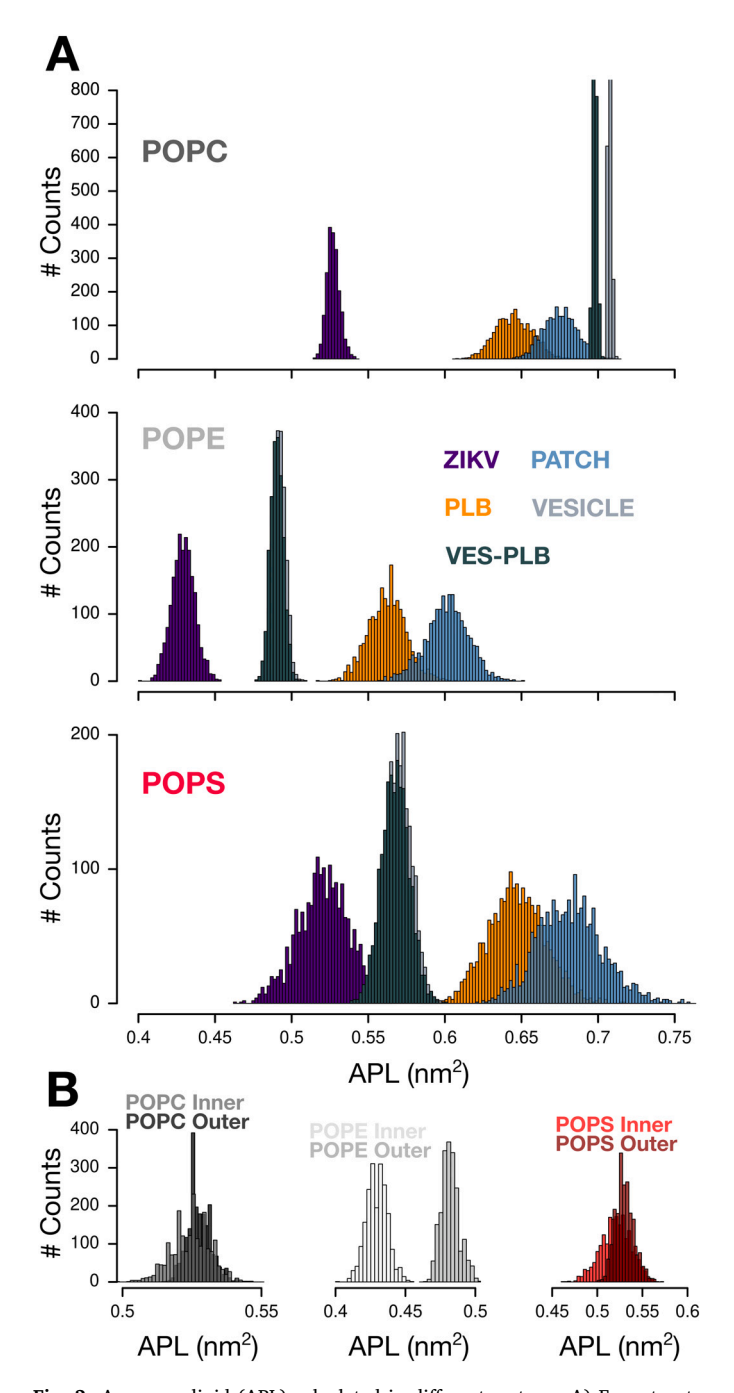


Fig. 3. Areas per lipid (APL) calculated in different systems. A) From top to bottom: POPC, POPE, and POPS. B) APLs for the three lipids in the ZIKV's VLP discriminating in inner and outer leaflets (lighter and darker colors, respectively).

However, the APL distributions of POPE and POPS in the inner side of the vesicle remained practically unchanged.

To provide a comparative estimation of the relevance of the curvature vs. protein-induced effects, we took profit from the fact that the three lipid species are present in both leaflets of the ZIKV system. Comparing the APLs in the inner and outer leaflets, we observe that, despite the convexity of the outer leaflet, POPC and POPS experience only small displacements to higher values (Fig. 3B). However, the smaller POPE's polar head size shows well-differentiated APL values and higher compaction in the inner leaflet. This behavior suggests that the quaternary effects imposed by the protein, rather than the curvature, dominate in shaping the viral membrane. Nevertheless, the negligible

impact of the six PLB copies on the APLs of the vesicle's inner leaflet may also suggest a role for the protein density to modulate protein-lipid compaction.

Unfortunately, calculations of compressibility or bending rigidity moduli are not trustworthy for the dimensions of the systems [56]. Moreover, the differences in thickness and curvature of the ZIKV membrane evidenced by CryoEM strongly suggest that assigning average values to biophysical properties may be misleading. Nevertheless, we sought to obtain a quantitative estimate for the lateral pressure exerted by viral quaternary structure on the membrane. Calculation of lateral pressures for spherical geometries is very challenging [57]. To the best of our knowledge, implementations for complex protein-lipid environments such as the Flavivirus envelopes are not currently available. Aimed to circumvent this problem, we performed a series of simulations on planar membrane patches progressively increasing the lateral pressure and monitored the APLs at each pressure. We reasoned that a lateral pressure producing the same APL measured in the VLP could provide a rough quantitative estimation of the pressure imposed by the virus. To this aim, we set up a flat patch containing only POPC, only POPE, and a symmetric POPC:POPE:POPS with 6:3:1 proportion (a patch made only of POPS was not stable because of electrostatic repulsion). The dimensions of those patches were comparable to the flat region observed in the CryoEM map of ZIKV (Fig. 1 [19]). Surprisingly, all three systems arrived at the point of rupture before reaching the ZIKV APL values. The pure POPC system broke at 31 bars attaining comparable APLs but with a wider distribution of values (Supplementary Fig. S2). The analogous POPE system resisted up to 66 bars. Although the distribution of APL values was comparable to that measured for ZIKV, the average values at the rupture pressure differ by nearly 0.03 nm² (Supplementary Fig. S3).

In contrast, the heterogeneous membrane patch showed an intermediate rupture pressure of 41 bar. Although the APL distributions for POPC and POPS were quite similar, the same value for POPE remained about 0.04 nm² higher in the planar system compared with the ZIKV (Figs. 4 and S4). Taken together, the data shown in Fig. 4 and S2-S4, we conclude that the intricate mesh of protein-protein interactions in the ZIKV exerts a highly stabilizing effect on the lipid bilayer. This stabilization allows achieving significant compaction in the membrane, which supports pressures beyond the point of rupture of an analogous flat membrane.

To gain further insights into the effect of the viral envelope on the bilayer, we calculated the number of lipid-lipid and lipid-protein contacts in the different systems studied. Aimed to facilitate the comparison, we normalized the lipid-lipid contacts to the total number of lipids in each scenario. In contrast, lipid-protein interactions were normalized by the number of $C\alpha$ carbons (see Methods). As shown in Fig. 5A, there are minor differences between the lipid-lipid contacts in the flat membrane patches. The presence of PLB in the flat membrane patch only slightly widens the gap between contacts in outer (cytoplasmic) and inner (ER luminal) lipids.

Nevertheless, the differences observed between the two leaflets may be mainly ascribed to homogeneous (POPC) vs. heterogeneous (POPE: POPS) distribution of membrane components. In line with this idea, a marked curvature of the membrane (as in the vesicle system) increases the difference in lipid-lipid contacts by nearly one unit per molecule, on average. A progressively more marked effect is observed for PLB in the vesicle and ZIKV, where both the curvature and the presence of the proteins produce a noticeable decrease in the lipid-lipid contacts (Fig. 5A).

We normalized the number of contacts by the number of $C\alpha$ carbons present in the different proteins to compare the effect of the three different protein environments analyzed. In the case of PLB, lipid contacts were calculated separately between the TM and cytoplasmic domains (named CH in Fig. 5B). In the case of ZIKV, lipid contacts were computed between the TM and stem (amphipathic) helices (Fig. 1A). As shown in Fig. 5B, the discrepancies between different helices are minor

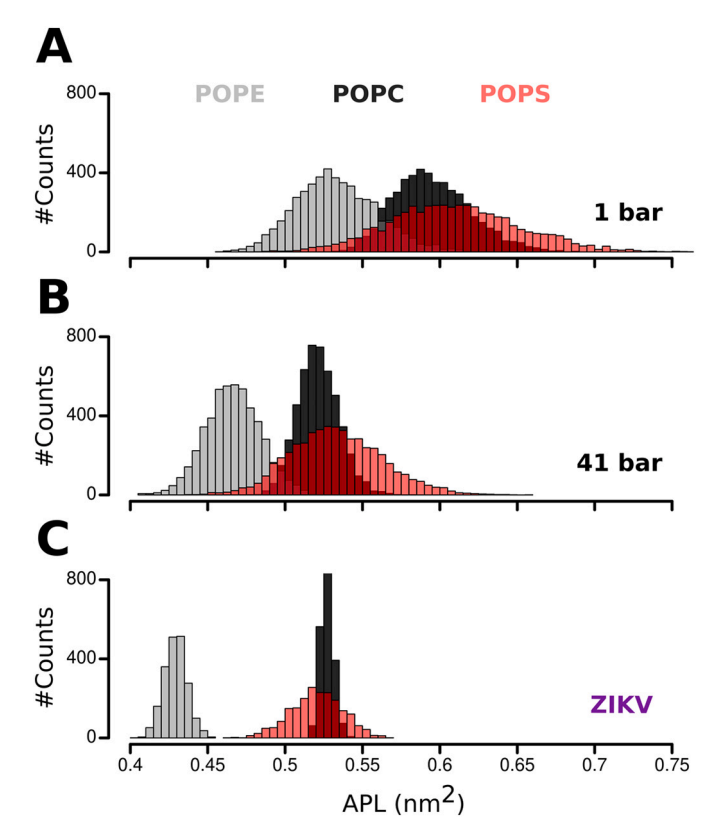


Fig. 4. Comparison between APLs in a flat patch at different lateral pressures vs. those in the VLP membrane. A) Histogram of APL values calculated on the different lipids during the simulation of the flat patch at 1 bar. B) Same as A for a flat patch under a lateral pressure of 41 bars (increasing this value leads to the disruption of the bilayer). C) APLs calculated on the VLP. These histograms correspond to the distributions presented in Fig. 3A and are provided here as a reference.

when comparing within the same system. However, the number of lipid-protein contacts in ZIKV exceeds those of the PLB in both systems independently of the leaflets. Strikingly, the average lipid-protein contacts increase by nearly one lipid per amino acid when going from the flat membrane to the vesicle and the VLP.

These stark differences originate in the intrinsic dynamics of each protein and the confinement imposed by the closed quaternary structure of the virus. Namely, the cytoplasmic helices of PLB alternate between states apposed to the membrane surface and fully solvent-exposed [37,41], while the rigidity of the ZIKV's ectodomain restraints the motion of the amphipathic helices to be in contact with the membrane surface (Fig. 1A). Moreover, the ZIKV's ectodomain forms a closed protein shell that severely impairs the solvent accessibility from the exterior, generating nanometer-sized solvent-filled cavities in contact with the outer leaflet (Fig. 1B).

On the opposite membrane side, the PLB's pentameric bundle of single-pass TM regions ends precisely at the membrane surface, exposing only the carboxylate moieties [37], creating a local concentration of negative charges that impairs the contacts with POPS. In contrast, we recently noted that ZIKV's double-pass TM helices present basic amino acids, absolutely conserved in all *Flaviviruses*, that create an electrostatically restrained annulus of acidic phospholipid at the inner leaflet in the proximity of the two-fold axis [31].

Since different interactions dictate the protein-lipid contacts, we examined the lipid's diffusion coefficients at both leaflets separately. Since proteins hamper lipid diffusion, and we are interested in characterizing the effect of the viral envelope on the membrane coat, we will only focus on a comparison between the PLB and ZIKV systems. As shown in Table 1, the lipids in the ZIKV's envelope showed a slower

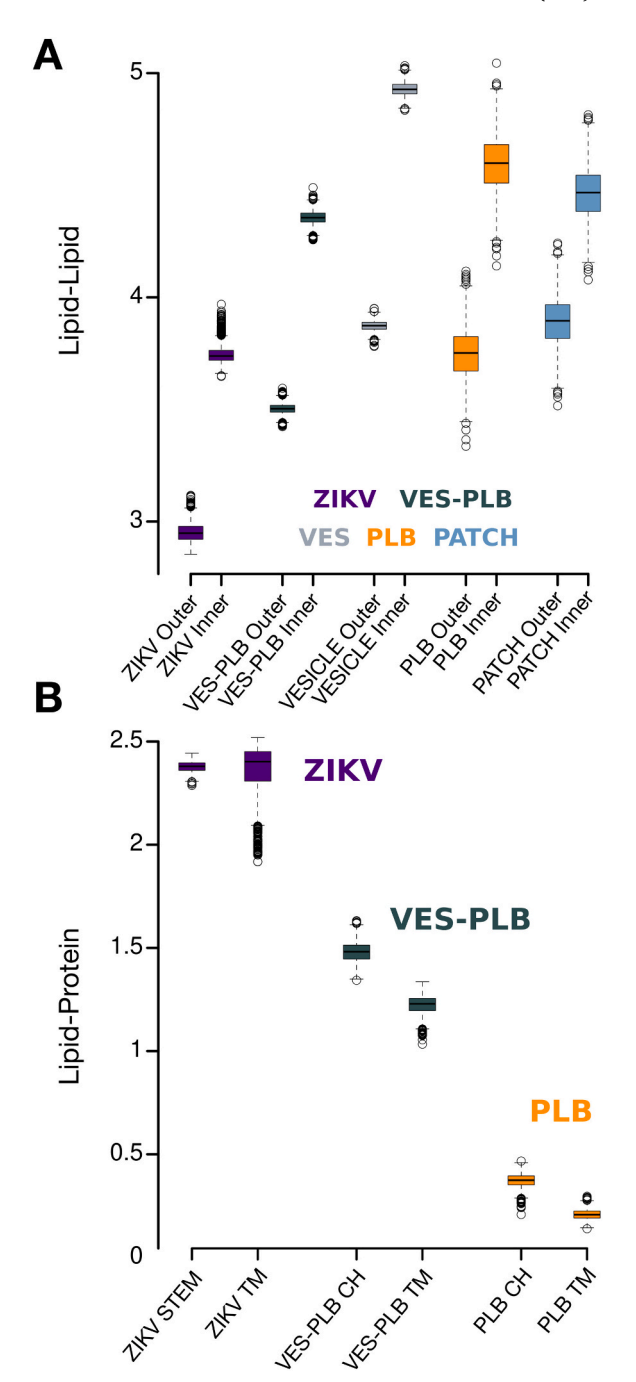


Fig. 5. Lipid-lipid and lipid-protein contacts. A) Lipid-lipid contacts among all three phospholipid species in all systems studied discriminated by membrane leaflet. The colors in the Box plots indicate the analyzed systems. Indigo: ZIKV, dark gray: Vesicle-PLB system, gray: Vesicle, orange: patch with PLB, and blue: flat patch bilayer. In the flat patch, outer and inner refer to leaflets containing only POPC and POPE:POPS, respectively. Contacts are normalized by the total number of lipids in each system. B) Lipid-protein contacts in the ZIKV, Vesicle-PLB, and flat membrane with PLB systems. Contacts were calculated between beads representing Glycerol and C α carbons. To facilitate the comparison, contacts are normalized by the number of C α carbons considered in each system. In PLB systems, CH indicates the cytoplasmic helices (solvent-exposed in Fig. 2C, E). (For interpretation of the references to color in this figure legend, the reader is referred to the web version of this article.)

Table 1 Diffusion coefficients ($\mu m^2/s$) per leaflet in PLB and ZIKV systems.

	ZIKV		PLB	
	Inner	Outer	ER lumen	Cytoplasm
POPC POPE POPS	$11 (\pm 5.5)$ $11 (\pm 6)$ $12 (\pm 6)$	9 (±7) 9 (±7) 9 (±8)	NA 14.2 (± 1.5) 14.6 ($\pm < 10^{-2}$)	21.8 (±0.8) NA NA

diffusion than those in the presence of PLB. We also measured a slight difference between both leaflets, suggesting slower diffusion values for all the lipids in the outer layer. However, the significant uncertainties associated with the measure make it challenging to reach a clear conclusion about the modulation of the long-range dynamics of the lipids in the viral envelope.

Aimed to dig further into this issue, we monitored the instantaneous displacement of phospholipids at the outer and inner sides of the viral membrane. Because of visualization convenience, we used one protein raft and selected all the lipids within 4 nm of any protein bead within that raft. These calculations provide a complementary vision to the diffusion coefficient. While the data presented in Table 1 were obtained from the mean square displacement of all lipids of the same species on the whole simulation time, the instantaneous displacement informs on the movement of each lipid (represented by arrowheads in Fig. 6) within a time window of 1 ns. In that sense, the information is to be taken as representative snapshots of the lipid displacement in one virus raft. The blank areas in Fig. 6 correspond to regions depleted of lipids, while the arrows are colored from blue to red to indicate slower and faster moving lipids, respectively. Arrowheads pointing in the directions of the displacement indicate the lipid's instantaneous positions. Although the snapshots in Fig. 6 depict a very short time window, the general features are conserved through the dynamics.

From a comparative view of the upper and lower panels, it is clear that the outer leaflet presents zones depleted from lipids. This is a direct effect of the presence of the amphipathic helices apposed onto the membrane surface. As the TM helices are not long enough to pass through the membrane completely, lipids cover almost the entire inner surface.

An evaluation of the instantaneous displacements in both leaflets showed that the inner lipids experience a faster movement (i.e., longer distances in the same time window). Moreover, there is no clear correspondence between lower and upper patterns, indicating that the motion in both leaflets is not correlated.

Aimed to characterize the decoupled dynamics of lipids in the viral membrane, we calculated the phospholipids' principal components of motion in the PLB and ZIKV systems according to the method proposed Buslaev et al. [53]. As CG lipids used in this study are composed of 16 (POPC and POPE) or 17 (POPS) effective beads, their motion can be decomposed in a space of $3\times N$ orthogonal dimensions, being N the number of beads. Our previous work reported an increased occupancy of POPS in the inner leaflet of ZIKV, around the TM helices, which contains highly conserved basic amino acids [31]. Therefore, comparing the principal components of the motion of POPS molecules may be informative of differential lipid-protein interactions in both leaflets. Hence, we will restrict our analysis to POPS because of the complexity of comparing multidimensional spaces for three lipids in two systems.

We calculated the covariance matrices of POPS and compared them in all cases, as their correlation indicates a similarity between their energy landscapes. The projection on the real space of the first five principal components, which account for 66% of the total variance in each case, is shown in Fig. 7A. The maximum and minimum amplitudes are indicated by blue and red colors, respectively. As it can be seen, the first mode mainly identifies a "scissoring" motion of the lipid tails, which is in agreement with several simulation results [53,58]. Although more intricate, only minor differences could be visually identified comparing the second to fifth principal components (Fig. 7A). Indeed, a comparison among the eigenvalues of the eigenvectors up to the ten principal components, shows negligible differences (Fig. 7B).

Hence, it becomes interesting to quantify the differences between the PCs in different systems. This can be obtained from the inner product between eigenvectors, which are shown in the checkered panels of Fig. 7C. Diagonal dark boxes indicate a good correspondence, while off-diagonal dark boxes imply a swapping of the eigenvectors in their relevance for the motion of each system. POPS in the PLB patch showed the best overlap with their counterparts in the outer leaflet of the VLP, while fewer diagonal patterns are observed in the other cases. Another quantitative comparison can be obtained from the correlation between covariance matrices. Considering only the first five principal components resulted in correlations higher than 93% regardless of the system and leaflet used in the comparison (see numbers in the lower corners of

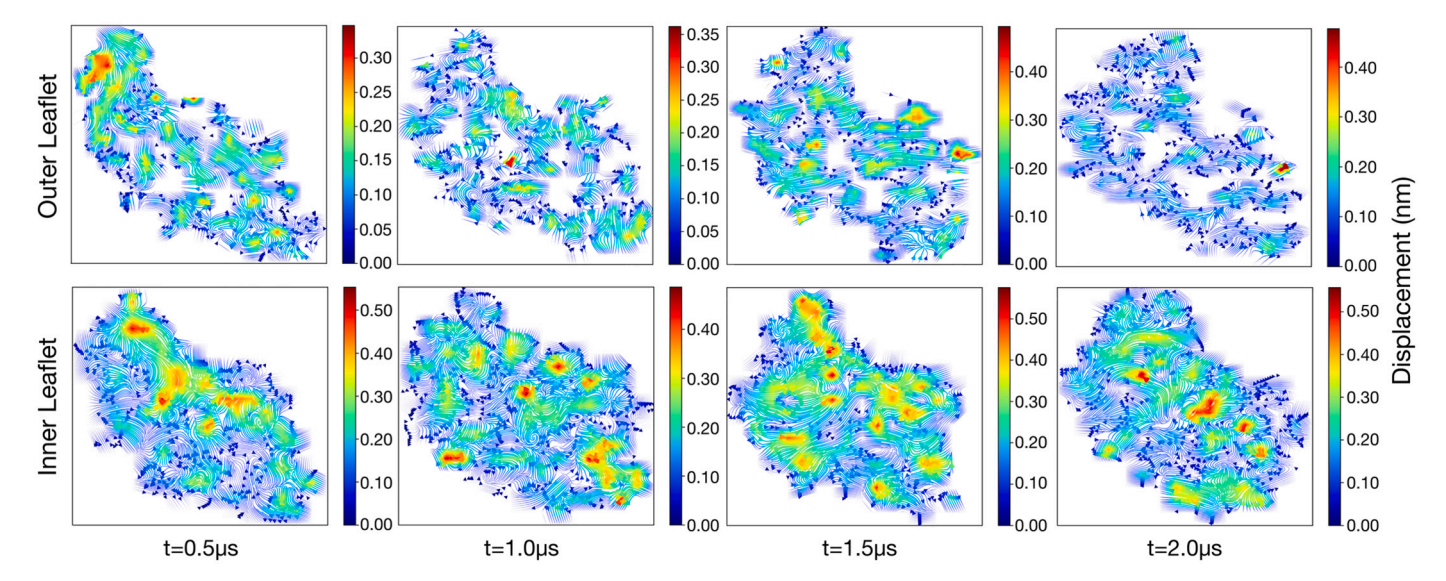


Fig. 6. Instantaneous displacement of lipids within 4 nm of a protein raft. Four representative snapshots along the dynamics are shown for the outer and inner leaflets (upper and lower rows, respectively). The pictures correspond to the same viewpoint on each leaflet. Arrowheads indicate the instantaneous position of phosphate moieties of individual phospholipids and point into the direction of the motion. The color scale is automatically adjusted in each panel to maximize the visualization of the whole range of displacements.

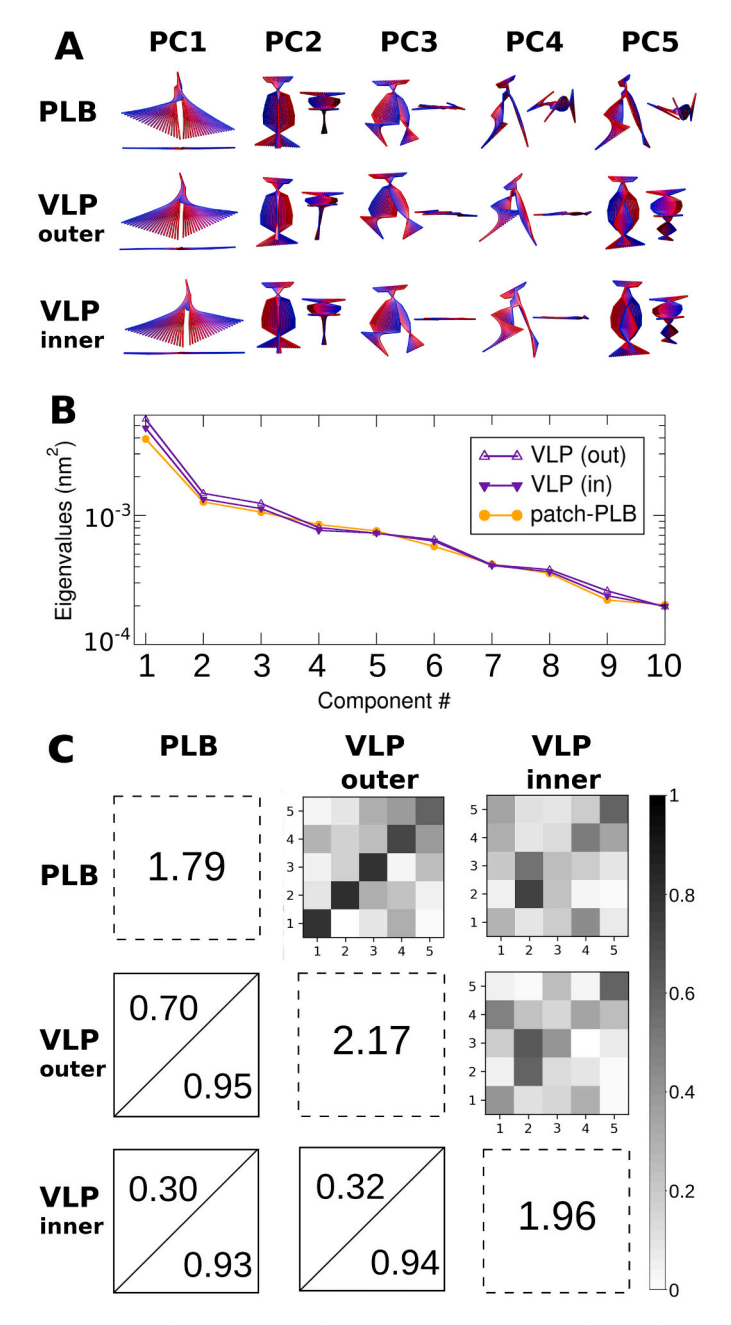


Fig. 7. Principal components analysis (PCA) of POPS in PLB in flat membrane and VLP systems. A) Projection of the principal components of the motion on the 3D space. Side and top views are shown for the first 5 PCs. B) Module of the eigenvalues as a function of the eigenvector number for the ten first principal components. C) Quantitative comparison of PCAs. Checkered panels illustrate the inner products between POPS in different systems for the first five eigenvectors. Numbers in the lower-left diagonal indicate the Pearson correlation (see Methods) between pairs of covariance matrices calculated using the entire matrices (upper numbers) or only the first five eigenvectors (lower numbers). The values reported in the diagonal indicate the respective traces of each covariance matrix.

off-diagonal boxes of Fig. 7C). This quantitative gauge is in line with the visual similarity among the principal modes shown in Fig. 7A. However, calculating the correlation of covariance matrices considering the whole matrix returned notably lower values, especially for the comparison between the inner VLP leaflet with the other two systems analyzed (numbers in the higher corners of off-diagonal boxes of Fig. 7C). This finding indicates that the higher motional components, associated with vibrational motion, accounted for most of the differences in the

dynamics of the lipids in different environments.

To characterize further this unexpected feature, we calculated the trace of the covariance matrices, which provides a quantitative gauge of the flexibility of each lipid. The traces of the covariance matrices are shown in the diagonal boxes of Fig. 7C. POPS in the outer VLP leaflet showed the maximum variance, supporting our idea that amphipathic helices perturb the normal dynamic behavior of phospholipids, i.e., reducing APL, and inducing new conformations. Since the main differences in the covariance matrices reside in the components associated with thermal fluctuations, the higher traces obtained for POPS in the outer leaflet suggest a decoupled dynamic and a role of the quaternary structure of the VLP in maintaining both leaflets in different energetic states.

4. Discussion and conclusions

The relevance of the cross-talk between proteins and lipids in physiopathological processes is widely recognized. In the specific context of viral infections, it is well established that viruses modulate the lipid production of infected cells and how this impacts infection and replication [59–61]. However, much less is known about the viral lipidomics in shaping the structure and dynamics of the viral particles. Because the dimensions of viral particles are in, or below, the lower limits of the resolution of the methods, computer simulations are progressively gaining momentum [62–64]. Indeed, computational virology can nowadays provide astonishing molecular details on complete viral particles [27].

Nevertheless, computational studies are not devoid of caveats. A frequently overlooked limitation of computational studies is the limited molecular repertoire incorporated in the simulations. However, remodeling of intracellular membranes is a crucial step to form viral replication sites in *Flaviviruses*. For example, ZIKV deregulates the sphingolipid balance of infected host cells redistributing ceramides to replication sites, and disruption of sphingolipid biosynthesis blocks ZIKV infection [65]. Conversely, WNV and DENV require different lipid mechanisms to replicate their genomes effectively. It has been shown that depletion of endogenous ceramide levels severely impairs WNV replication, while the same treatment exerts a potentiating effect on DENV [66].

Another critical component is Cholesterol, which has been shown to play important roles at different points of the replication cycle of other *Flaviviruses* [67,68]. The vast complexity introduced by the considerable variability in membrane components is highly challenging and a limitation to keep in mind to assign the proper weight to computational studies.

Aimed to contribute new insights into the role of lipid-protein interactions in the context of a viral envelope, we undertook the analysis of structural and dynamical properties of lipids and lipid-protein interactions on an entire ZIKV VLP by performing CG molecular dynamics simulations. To establish a proper reference, the simulation of the VLP was compared with simpler molecular systems as a flat membrane patch and a small vesicle, in the presence and absence of the ER pentameric protein PLB. The differences observed highlight the relevance of performing molecular simulations in the correct biophysical environment.

Our study included the three more abundant lipid species present in the ER, namely POPC, POPE, and POPS in a 6:3:1 proportion. Since information about the distribution of lipids in the viral envelope is not available, we assumed the three species to be symmetrically distributed in both leaflets. While the possible modulation of biophysical properties by different sphingolipids is difficult to estimate, we would expect limited effects associated with the presence of Cholesterol. Indeed, Cholesterol constitutes about 5% of the lipid content of the ER membrane [69,70], and has been reported to increase nearly a 50% in ZIKV infected cells [65]. However, experimental and simulation studies report limited alterations in the biophysical properties of bilayers upon addition of up to nearly 10% of Cholesterol [56,71]. On the other hand, very

recent high-resolution structures of different *Flaviviruses* have identified the presence of lipid pockets in the neighborhood of the TM and Stem helices of E and M proteins [72,73]. Although the resolution is barely enough to speculate about the identity of specific lipids, the lipid's electronic densities certainly don't match to Cholesterol molecules, suggesting at least that no unmistakable fingerprints for Cholesterol are present in the close neighborhood of the TM part of the protein.

Despite these differences with the experimental conditions, it is important to point out that our simulation setup reproduced with remarkable accuracy the CryoEM structure of the entire VLP and that of the membrane region (Supplementary Fig. S1). These facts suggest that the lateral pressures exerted on the phospholipids are, at least, in the correct range. An accurate description of the system's pressure is crucial because "the concentration of large interfacial free energies within the microscopically narrow region, as in a monolayer or bilayer film, leads to enormous local lateral pressure densities corresponding to bulk pressures of hundreds of atmospheres or more" [74]. Although calculating lateral (or rather, tangential) pressures in a closed and heterogenous system as the ZIKV VPL is complicated, we sorted out to evaluate a direct effect, namely, the areas per lipid. Comparison of APLs showed that lipids in the viral envelope bear a considerable lateral pressure, shrinking to about 30% of the values measured in the flat membrane patch (Fig. 3A). These are substantial compaction values considering that APL shrinkages in the order of 10% have been reported from MD simulations upon adding as much as 1 M NaCl to POPC/POPS mixtures [75]. Similarly, 2HNMR spectroscopy experiments showed a 17% area contraction upon dehydration in DMPC mixes [76]. A series of simulations progressively increasing the lateral pressure on flat bilayers suggests a lower estimate of nearly 40 bars for the lipids in the viral envelope.

Another remarkable outcome of our study is the asymmetry in the dynamics and energetics encountered between the phospholipids in the two leaflets of the viral membrane. Although the CryoEM structures of this and other *Flaviviruses* clearly show a marked asymmetry in the solvent accessibility [77,78], this issue had not been characterized in detail to our knowledge. The integration of our results with the growing number of structures of *Flaviviruses* reported suggests that the extreme compaction and asymmetric properties may not only result from discrete interactions with the viral proteins but rather from the restrictions imposed by the quaternary structure as a whole. In contrast to the extensive solvation in the inner layer, the presence of small solvent-filled regions in contact with the outer leaflet most likely creates an unbalance in the viral envelope. This implies that substantial tensile energy is stored in the mature viral membrane.

Flaviviruses replicate and assemble in the ER to then transit through the Golgi apparatus to finally bud off. Along their path, they suffer pH variations and proteolytic cleavage adopting "bumpy" and "smooth" shapes that necessarily require the membrane's plasticity to keep the genetic material sealed from the exterior [35]. Our observations suggest that a large plasticity can be easily achieved by the virion, as the membrane components can expand nearly 30% without compromising the shielding of the genetic material. Once in the mature form, the virion remains in a high-energy state that triggers at low pH in the host cell's late endosome [79,80]. The pH triggering involves a conformational transition in which E-M heterodimers dissociate to form trimeric fusion spikes [81]. The membrane stress can provide the energy needed to detach the amphipathic stem helices from the membrane [82,83] or overcome the first barrier associated with membrane fusion, namely, desolvation and formation of a lipid stalk [84,85], or both. Regardless of the case, our study suggests shifting from a protein-centric model of fusion activation to a scheme where the membrane plays a more active role in flaviviral fusion.

Declaration of competing interest

The authors declare that they have no known competing financial interests or personal relationships, which have or could be perceived to

have influenced the work reported in this article.

Data availability

Data will be made available on request.

Acknowledgments

This work was partially funded by FOCEM (MERCOSUR Structural Convergence Fund), COF 03/11. EEB and SP belong to the SNI program of ANII. EEB was a beneficiary of a postdoctoral fellowship of CONICET. MS is the beneficiary of a Ph.D. fellowship of ANII. Molecular dynamics simulations were performed at the Uruguayan Supercomputer Center ClusterUY. We highly appreciated valuable discussions with Dr. Leonel "lipid lover" Malacrida.

Appendix A. Supplementary data

Supplementary data to this article can be found online at https://doi.org/10.1016/j.bbamem.2021.183804.

References

- J.F. Danielli, H. Davson, A contribution to the theory of permeability of thin films, J. Cell. Comp. Physiol. 5 (1935), https://doi.org/10.1002/jcp.1030050409.
- [2] S.J. Singer, G.L. Nicolson, The fluid mosaic model of the structure of cell membranes, Science 175 (1972), https://doi.org/10.1126/science.175.4023.720.
- [3] A.W. Smith, Lipid-protein interactions in biological membranes: a dynamic perspective 1818 (2012), https://doi.org/10.1016/j.bbamem.2011.06.015.
- [4] Z. Cournia, T.W. Allen, I. Andricioaei, B. Antonny, D. Baum, G. Brannigan, N.-V. Buchete, J.T. Deckman, L. Delemotte, C. del Val, R. Friedman, P. Gkeka, H.-C. Hege, J. Hénin, M.A. Kasimova, A. Kolocouris, M.L. Klein, S. Khalid, M. J. Lemieux, N. Lindow, M. Roy, J. Selent, M. Tarek, F. Tofoleanu, S. Vanni, S. Urban, D.J. Wales, J.C. Smith, A.-N. Bondar, Membrane protein structure, function, and dynamics: a perspective from experiments and theory, J. Membr. Biol. 248 (2015), https://doi.org/10.1007/s00232-015-9802-0.
- [5] G.L. Nicolson, The Fluid—Mosaic Model of Membrane Structure: Still relevant to understanding the structure, function and dynamics of biological membranes after more than 40years 1838 (2014), https://doi.org/10.1016/j.bbamem.2013.10.019.
- [6] Y. Sako, A. Kusumi, Compartmentalized structure of the plasma membrane for receptor movements as revealed by a nanometer-level motion analysis, J. Cell Biol. 125 (1994), https://doi.org/10.1083/jcb.125.6.1251.
- [7] K. Jørgensen, J.H. Ipsen, O.G. Mouritsen, Chapter 2 lipid-bilayer heterogeneity, in: Principles of Medical Biology 7, 1997, pp. 19–38, https://doi.org/10.1016/S1569-2582(97)80083-9.
- [8] H.-Y. Wang, D. Bharti, I. Levental, Membrane heterogeneity beyond the plasma membrane, Front. Cell Dev. Biol. (2020) 1186, https://doi.org/10.3389/ FCELL.2020.580814.
- [9] D. Lingwood, H.-J. Kaiser, I. Levental, K. Simons, Lipid rafts as functional heterogeneity in cell membranes, Biochem. Soc. Trans. 37 (2009) 955–960, https://doi.org/10.1042/BST0370955.
- [10] K. Simons, G. van Meer, Lipid sorting in epithelial cells, Biochemistry 27 (2002) 6197–6202, https://doi.org/10.1021/BI00417A001.
- [11] K. Simons, J.L. Sampaio, Membrane organization and lipid rafts, Cold Spring Harb. Perspect. Biol. 3 (2011), a004697, https://doi.org/10.1101/CSHPERSPECT. A004697
- [12] F.M. Goñi 1838 (2014) 1467–1476, https://doi.org/10.1016/J. BBAMEM.2014.01.006.
- [13] E. Sezgin, Super-resolution optical microscopy for studying membrane structure and dynamics, J. Phys. Condens. Matter 29 (2017), 273001, https://doi.org/ 10.1088/1361-648X/AA7185.
- [14] K. Zhanghao, W. Liu, M. Li, Z. Wu, X. Wang, X. Chen, C. Shan, H. Wang, X. Chen, Q. Dai, P. Xi, D. Jin, High-dimensional super-resolution imaging reveals heterogeneity and dynamics of subcellular lipid membranes, Nat. Commun. 11 (1) (2020), https://doi.org/10.1038/s41467-020-19747-0, 1-10.
- [15] M.B. Stone, S.A. Shelby, S.L. Veatch, Super-resolution microscopy: shedding light on the cellular plasma membrane, Chem. Rev. 117 (2017) 7457–7477, https://doi. org/10.1021/ACS.CHEMREV.6B00716.
- [16] E. Arauz, V. Aggarwal, A. Jain, T. Ha, J. Chen, Single-molecule analysis of lipid-protein interactions in crude cell lysates, Anal. Chem. 88 (2016) 4269–4276, https://doi.org/10.1021/ACS.ANALCHEM.5B04127.
- [17] S.J. Opella, F.M. Marassi, Applications of NMR to membrane proteins, Arch. Biochem. Biophys. 628 (2017) 92–101, https://doi.org/10.1016/J. ABB.2017.05.011.
- [18] D. Huster, Solid-state NMR spectroscopy to study protein-lipid interactions 1841 (2014) 1146–1160, https://doi.org/10.1016/J.BBALIP.2013.12.002.
- [19] M. Sevvana, F. Long, A.S. Miller, T. Klose, G. Buda, L. Sun, R.J. Kuhn, M. G. Rossmann, Refinement and analysis of the mature Zika virus cryo-EM structure

- at 3.1 Å resolution, Structure 26 (2018) 1169–1177.e3, https://doi.org/10.1016/J.
- [20] S. Welsch, S. Miller, I. Romero-Brey, A. Merz, C.K.E. Bleck, P. Walther, S.D. Fuller, C. Antony, J. Krijnse-Locker, R. Bartenschlager, Composition and three-dimensional architecture of the dengue virus replication and assembly sites, Cell Host Microbe 5 (2009) 365–375, https://doi.org/10.1016/J.CHOM.2009.03.007.
- [21] M. Chavent, A.L. Duncan, M.S.P. Sansom, Molecular dynamics simulations of membrane proteins and their interactions: from nanoscale to mesoscale, Curr. Opin. Struct. Biol. 40 (2016) 8–16, https://doi.org/10.1016/J.SBI.2016.06.007.
- [22] L. Saiz, M.L. Klein, Computer simulation studies of model biological membranes, Acc. Chem. Res. 35 (2002), https://doi.org/10.1021/ar010167c.
- [23] S.J. Marrink, V. Corradi, P.C.T. Souza, H.I. Ingólfsson, D.P. Tieleman, M.S. P. Sansom, Computational modeling of realistic cell membranes, Chem. Rev. 119 (2019) 6184–6226, https://doi.org/10.1021/ACS.CHEMREV.8B00460.
- [24] S. Pöyry, I. Vattulainen, Role of charged lipids in membrane structures insight given by simulations 1858 (2016) 2322–2333, https://doi.org/10.1016/J. BBAMEM.2016.03.016.
- [25] M.P. Muller, T. Jiang, C. Sun, M. Lihan, S. Pant, P. Mahinthichaichan, A. Trifan, E. Tajkhorshid, Characterization of lipid-protein interactions and lipid-mediated modulation of membrane protein function through molecular simulation, Chem. Rev. 119 (2019) 6086–6161, https://doi.org/10.1021/ACS.CHEMREV.8B00608.
- [26] A. Barducci, M. Bonomi, M. Parrinello, Metadynamics 1 (2011) 826–843, https://doi.org/10.1002/WCMS.31.
- [27] M.R. Machado, S. Pantano, Fighting viruses with computers, right now, Curr. Opin. Virol. 48 (2021) 91–99, https://doi.org/10.1016/J.COVIRO.2021.04.004.
- [28] T. Reddy, D. Shorthouse, D.L. Parton, E. Jefferys, P.W. Fowler, M. Chavent, M. Baaden, M.S.P. Sansom, Nothing to sneeze at: a dynamic and integrative computational model of an influenza a virion, Structure 23 (2015) 584–597, https://doi.org/10.1016/J.STR.2014.12.019.
- [29] T. Reddy, M.S.P. Sansom, The role of the membrane in the structure and biophysical robustness of the dengue virion envelope, Structure 24 (2016) 375–382, https://doi.org/10.1016/J.STR.2015.12.011.
- [30] A. Yu, A.J. Pak, P. He, V. Monje-Galvan, L. Casalino, Z. Gaieb, A.C. Dommer, R. E. Amaro, G.A. Voth, A multiscale coarse-grained model of the SARS-CoV-2 virion, Biophys. J. 120 (2021) 1097–1104, https://doi.org/10.1016/J.BPJ.2020.10.048.
- [31] M. Soñora, L. Martínez, S. Pantano, M.R. Machado, Wrapping up viruses at multiscale resolution: optimizing PACKMOL and SIRAH execution for simulating the zika virus, J. Chem. Inf. Model. 61 (2021) 408–422, https://doi.org/10.1021/ ACS_ICIM_0C01205
- [32] M.R. Machado, H.C. González, S. Pantano, MD simulations of viruslike particles with supra CG solvation affordable to desktop computers, J. Chem. Theory Comput. 13 (2017) 5106–5116, https://doi.org/10.1021/ACS.JCTC.7B00659.
- [33] A. Marcello, S. Pantano, Interdisciplinary approaches to the study of flavivirus, Biochem. Biophys. Res. Commun. 492 (2017) 531–532, https://doi.org/10.1016/ J.BBRC.2017.08.099.
- [34] W. Zhang, B. Kaufmann, P.R. Chipman, R.J. Kuhn, M.G. Rossmann, Membrane curvature in flaviviruses, J. Struct. Biol. 183 (2013) 86–94, https://doi.org/ 10.1016/J.JSB.2013.04.005
- [35] R.J. Kuhn, K.A. Dowd, C.Beth Post, T.C. Pierson, Shake, rattle, and roll: Impact of the dynamics of flavivirus particles on their interactions with the host, Virology 479–480 (2015) 508–517, https://doi.org/10.1016/J.VIROL.2015.03.025.
- [36] S. Pantano, E. Carafoli, The role of phosphorylation on the structure and dynamics of phospholamban: a model from molecular simulations 66 (2007) 930–940, https://doi.org/10.1002/PROT.21239.
- [37] R. Verardi, L. Shi, N.J. Traaseth, N. Walsh, G. Veglia, Structural topology of phospholamban pentamer in lipid bilayers by a hybrid solution and solid-state NMR method, Proc. Natl. Acad. Sci. 108 (2011) 9101–9106, https://doi.org/ 10.1073/PNAS.1016535108.
- [38] E.E. Barrera, M.R. Machado, S. Pantano, Fat SIRAH: coarse-grained phospholipids to explore membrane-protein dynamics, J. Chem. Theory Comput. 15 (2019) 5674–5688, https://doi.org/10.1021/ACS.JCTC.9B00435.
- [39] J.K. Marzinek, D.A. Holdbrook, R.G. Huber, C. Verma, P.J. Bond, Pushing the envelope: dengue viral membrane coaxed into shape by molecular simulations, Structure 24 (2016) 1410–1420, https://doi.org/10.1016/J.STR.2016.05.014.
- [40] J.K. Marzinek, R.G. Huber, P.J. Bond, Multiscale modelling and simulation of viruses, Curr. Opin. Struct. Biol. 61 (2020) 146–152, https://doi.org/10.1016/J. SBI.2019.12.019.
- [41] M.R. Machado, E.E. Barrera, F. Klein, M. Sóñora, S. Silva, S. Pantano, The SIRAH 2.0 force field: altius, fortius, citius, J. Chem. Theory Comput. 15 (2019) 2719–2733, https://doi.org/10.1021/ACS.JCTC.9B000006.
- [42] R. Capelli, A. Gardin, C. Empereur-mot, G. Doni, G.M. Pavan, A data-driven dimensionality reduction approach to compare and classify lipid force fields, J. Phys. Chem. B 125 (2021) 7785–7796, https://doi.org/10.1021/ACS. JPCB 1002503
- [43] M.R. Machado, S. Pantano, SIRAH tools: mapping, backmapping and visualization of coarse-grained models, Bioinformatics 32 (2016) 1568–1570, https://doi.org/ 10.1093/BIOINFORMATICS/BTW020.
- [44] G. Bussi, D. Donadio, M. Parrinello, Canonical sampling through velocity rescaling, J. Chem. Phys. 126 (2007), 014101, https://doi.org/10.1063/1.2408420.
- [45] M. Parrinello, A. Rahman, Polymorphic transitions in single crystals: a new molecular dynamics method, J. Appl. Phys. 52 (1998) 7182, https://doi.org/ 10.1063/1.328693.
- [46] L. Martínez, R. Andrade, E.G. Birgin, J.M. Martínez, PACKMOL: a package for building initial configurations for molecular dynamics simulations, J. Comput. Chem. 30 (2009) 2157–2164, https://doi.org/10.1002/JCC.21224.

- [47] H.J.C. Berendsen, J.P.M. Postma, W.F. van Gunsteren, A. DiNola, J.R. Haak, Molecular dynamics with coupling to an external bath, J. Chem. Phys. 81 (1998) 3684, https://doi.org/10.1063/1.448118.
- [48] M.J. Abraham, D. van der Spoel, E. Lindahl, B. Hess, GROMACS Development Team, GROMACS User Manual Version 2018, 2018. www.Gromacs.Org.
- [49] S. Páll, M.J. Abraham, C. Kutzner, B. Hess, E. Lindahl, in: Tackling Exascale Software Challenges in Molecular Dynamics Simulations with GROMACS, Lecture Notes in Computer Science (Including Subseries Lecture Notes in Artificial Intelligence and Lecture Notes in Bioinformatics) 8759, 2014, pp. 3–27, https:// doi.org/10.1007/978-3-319-15976-8 1.
- [50] Q. Zhang, C. Hunke, Y.H. Yau, V. Seow, S. Lee, L.B. Tanner, X.L. Guan, M.R. Wenk, G. Fibriansah, P.L. Chew, P. Kukkaro, G. Biuković, P.Y. Shi, S.G. Shochat, G. Grüber, S.M. Lok, The stem region of premembrane protein plays an important role in the virus surface protein rearrangement during dengue maturation, J. Biol. Chem. 287 (2012) 40525–40534, https://doi.org/10.1074/JBC.M112.384446.
- [51] H.M. Hankins, R.D. Baldridge, P. Xu, T.R. Graham, Role of flippases, scramblases and transfer proteins in phosphatidylserine subcellular distribution, Traffic 16 (2015) 35–47, https://doi.org/10.1111/TRA.12233.
- [52] S. Buchoux, FATSLiM: a fast and robust software to analyze MD simulations of membranes, Bioinformatics 33 (2017) 133–134, https://doi.org/10.1093/ BIOINFORMATICS/BTW563.
- [53] P. Buslaev, V. Gordeliy, S. Grudinin, I. Gushchin, Principal component analysis of lipid molecule conformational changes in molecular dynamics simulations, J. Chem. Theory Comput. 12 (2016) 1019–1028, https://doi.org/10.1021/ACS. ICCC 5801106
- [54] W. Humphrey, A. Dalke, K. Schulten, VMD: visual molecular dynamics, J. Mol. Graph. 14 (1996) 33–38, https://doi.org/10.1016/0263-7855(96)00018-5.
- [55] M. Chavent, T. Reddy, J. Goose, A.C.E. Dahl, J.E. Stone, B. Jobard, M.S.P. Sansom, Methodologies for the analysis of instantaneous lipid diffusion in md simulations of large membrane systems, Faraday Discuss. 169 (2014) 455–475, https://doi.org/ 10.1039/C3FD00145H
- [56] J. Eid, H. Razmazma, A. Jraij, A. Ebrahimi, L. Monticelli, On calculating the bending modulus of lipid bilayer membranes from buckling simulations, J. Phys. Chem. B 124 (2020) 6299–6311, https://doi.org/10.1021/ACS.JPCB.0C04253.
- [57] D.A. Grillo, J.M.R. Albano, E.E. Mocskos, J.C. Facelli, M. Pickholz, M.B. Ferraro, Mechanical properties of drug loaded diblock copolymer bilayers: a molecular dynamics study, J. Chem. Phys. 148 (2018), 214901, https://doi.org/10.1063/ 1.5028377.
- [58] P. Buslaev, I. Gushchin, Effects of coarse graining and saturation of hydrocarbon chains on structure and dynamics of simulated lipid molecules, Sci. Rep. 7 (1) (2017), https://doi.org/10.1038/s41598-017-11761-5, 1-15.
- [59] M. Mazzon, J. Mercer, Lipid interactions during virus entry and infection, Cell. Microbiol. 16 (2014) 1493–1502, https://doi.org/10.1111/CMI.12340.
- [60] N.S. Heaton, G. Randall, Multifaceted roles for lipids in viral infection, Trends Microbiol. 19 (2011) 368–375. https://doi.org/10.1016/J.TIM.2011.03.007.
- [61] E. Ketter, G. Randall, in: Virus Impact on Lipids and Membranes 6, 2019, pp. 319–340, https://doi.org/10.1146/ANNUREV-VIROLOGY-092818-015748.
- [62] J.K. Marzinek, R.G. Huber, P.J. Bond, Multiscale modelling and simulation of viruses, Curr. Opin. Struct. Biol. 61 (2020) 146–152, https://doi.org/10.1016/J. SBI 2019 12 019
- [63] E.E. Jefferys, M.S.P. Sansom, Computational virology: molecular simulations of virus dynamics and interactions, Adv. Exp. Med. Biol. 1140 (2019) 201–233, https://doi.org/10.1007/978-3-030-14741-9 10.
- [64] J.A. Hadden, J.R. Perilla, All-atom virus simulations, Curr. Opin. Virol. 31 (2018) 82–91, https://doi.org/10.1016/J.COVIRO.2018.08.007.
- [65] H.C. Leier, J.B. Weinstein, J.E. Kyle, J.-Y. Lee, L.M. Bramer, K.G. Stratton, D. Kempthorne, A.R. Navratil, E.G. Tafesse, T. Hornemann, W.B. Messer, E. A. Dennis, T.O. Metz, E. Barklis, F.G. Tafesse, A global lipid map defines a network essential for Zika virus replication, Nat. Commun. 11 (1) (2020), https://doi.org/ 10.1038/s41467-020-17433-9, 1–15.
- [66] T.E. Aktepe, H. Pham, J.M. Mackenzie, Differential utilisation of ceramide during replication of the flaviviruses West Nile and dengue virus, Virology 484 (2015) 241–250, https://doi.org/10.1016/J.VIROL.2015.06.015.
- [67] J.F. Osuna-Ramos, J.M. Reyes-Ruiz, R.M. del Ángel, The role of host cholesterol during flavivirus infection, Front. Cell. Infect. Microbiol. (2018) 388, https://doi. org/10.3389/FCIMB.2018.00388.
- [68] M.A. Martín-Acebes, Á. Vázquez-Calvo, J.C. Saiz, Lipids and flaviviruses, present and future perspectives for the control of dengue, zika, and West Nile viruses, Prog. Lipid Res. 64 (2016) 123–137, https://doi.org/10.1016/J.PLIPRES.2016.09.005.
- [69] A. Radhakrishnan, J.L. Goldstein, J.G. McDonald, M.S. Brown, Switch-like control of SREBP-2 transport triggered by small changes in ER cholesterol: a delicate balance, Cell Metab. 8 (2008) 512–521, https://doi.org/10.1016/J. CMRT 2008 10.008
- [70] A. Sokolov, A. Radhakrishnan, Accessibility of cholesterol in endoplasmic reticulum membranes and activation of SREBP-2 switch abruptly at a common cholesterol threshold, J. Biol. Chem. 285 (2010) 29480–29490, https://doi.org/ 10.1074/JBC_M110.148254.
- [71] R. Krivanek, L. Okoro, R. Winter, Effect of cholesterol and ergosterol on the compressibility and volume fluctuations of phospholipid-sterol bilayers in the critical point region: a molecular acoustic and calorimetric study, Biophys. J. 94 (2008) 3538–3548, https://doi.org/10.1529/BIOPHYSJ.107.122549.
- [72] B. Khare, T. Klose, Q. Fang, M.G. Rossmann, R.J. Kuhn, Structure of usutu virus SAAR-1776 displays fusion loop asymmetry, Proc. Natl. Acad. Sci. 118 (2021), e2107408118, https://doi.org/10.1073/PNAS.2107408118.
- [73] J.M. Hardy, N.D. Newton, N. Modhiran, C.A.P. Scott, H. Venugopal, L.J. Vet, P. R. Young, R.A. Hall, J. Hobson-Peters, F. Coulibaly, D. Watterson, A unified route

- for flavivirus structures uncovers essential pocket factors conserved across pathogenic viruses, Nat. Commun. 12 (1) (2021), https://doi.org/10.1038/s41467-021-22773-1, 1–13.
- [74] R.S. Cantor, Lateral pressures in cell membranes: a mechanism for modulation of protein function, J. Phys. Chem. B 101 (1997) 1723–1725, https://doi.org/ 10.1021/IP963911X
- [75] P. Jurkiewicz, L. Cwiklik, A. Vojtíšková, P. Jungwirth, M. Hof 1818 (2012) 609–616, https://doi.org/10.1016/J.BBAMEM.2011.11.033.
- [76] J.J. Kinnun, K.J. Mallikarjunaiah, H.I. Petrache, M.F. Brown, Elastic deformation and area per lipid of membranes: atomistic view from solid-state deuterium NMR spectroscopy 1848 (2015) 246–259, https://doi.org/10.1016/J. BBAMEM.2014.06.004.
- [77] T. Füzik, P. Formanová, D. Růžek, K. Yoshii, M. Niedrig, P. Plevka, Structure of tick-borne encephalitis virus and its neutralization by a monoclonal antibody, Nature Communications 9 (1) (2018), https://doi.org/10.1038/s41467-018-02882-0. 1–15.
- [78] X. Wang, S.-H. Li, L. Zhu, Q.-G. Nian, S. Yuan, Q. Gao, Z. Hu, Q. Ye, X.-F. Li, D.-Y. Xie, N. Shaw, J. Wang, T.S. Walter, J.T. Huiskonen, E.E. Fry, C.-F. Qin, D. I. Stuart, Z. Rao, Near-atomic structure of Japanese encephalitis virus reveals critical determinants of virulence and stability, Nat. Commun. 8 (1.) (2017), https://doi.org/10.1038/s41467-017-00024-6, 1–9.
- [79] J.M. Smit, B. Moesker, I. Rodenhuis-Zybert, J. Wilschut, Flavivirus cell entry and membrane fusion, Viruses 3 (2011) 160–171, https://doi.org/10.3390/V3020160.

- [80] K. Stiasny, R. Fritz, K. Pangerl, F.X. Heinz, Molecular mechanisms of flavivirus membrane fusion, Amino Acids 41 (5) (2009) 1159–1163, https://doi.org/ 10.1007/S00726-009-0370-4.
- [81] S. Bressanelli, K. Stiasny, S.L. Allison, E.A. Stura, S. Duquerroy, J. Lescar, F. X. Heinz, F.A. Rey, Structure of a flavivirus envelope glycoprotein in its low-pH-induced membrane fusion conformation, EMBO J. 23 (2004) 728–738, https://doi.org/10.1038/SJ.EMBOJ.7600064.
- [82] P. Guardado-Calvo, K. Atkovska, S.A. Jeffers, N. Grau, M. Backovic, J. Pérez-Vargas, S.M. de Boer, M.A. Tortorici, G. Pehau-Arnaudet, J. Lepault, P. England, P. J. Rottier, B.J. Bosch, J.S. Hub, F.A. Rey, A glycerophospholipid-specific pocket in the RVFV class II fusion protein drives target membrane insertion, Science 358 (2017) 663–667, https://doi.org/10.1126/SCIENCE.AAL.2712.
- [83] V. Nayak, M. Dessau, K. Kucera, K. Anthony, M. Ledizet, Y. Modis, Crystal structure of dengue virus type 1 envelope protein in the postfusion conformation and its implications for membrane fusion, J. Virol. 83 (2009) 4338–4344, https://doi.org/ 10.1128/JVI.02574-08
- [84] Y.G. Smirnova, M. Müller, How does curvature affect the free-energy barrier of stalk formation? Small vesicles vs apposing, planar membranes, Eur. Biophys. J. 50 (2021) 253–264, https://doi.org/10.1007/S00249-020-01494-1.
- [85] Y. Kozlovsky, M.M. Kozlov, Stalk model of membrane fusion: solution of energy crisis, Biophys. J. 82 (2002) 882–895, https://doi.org/10.1016/S0006-3495(02) 75450-7